Cellular/Molecular

Differential Coassembly of α1-GABA$_A$Rs Associated with Epileptic Encephalopathy

Saad Hannan,[1] Aida H.B. Affandi,[1] Marielle Minere,[1] Charlotte Jones,[1] Pollyanna Goh,[2] Gary Warnes,[2] Bernt Popp,[3,4] Regina Trollmann,[5] Dean Nizetic,[2,6] and Trevor G. Smart[1]

[1]Department of Neuroscience, Physiology and Pharmacology, University College London, London, WC1E 6BT, United Kingdom, [2]The Blizard Institute, Barts & The London School of Medicine, Queen Mary University of London, London, E1 2AT, United Kingdom, [3]Institute of Human Genetics, University Hospital Erlangen, Friedrich-Alexander-Universität Erlangen-Nürnberg, Erlangen, 91054, Germany, [4]Institute of Human Genetics, University of Leipzig Hospitals and Clinics, Leipzig, 04103, Germany, [5]Department of Pediatrics, Division of Neuropediatrics, Friedrich-Alexander-Universität Erlangen-Nürnberg, Erlangen, 91054, Germany, and [6]Lee Kong Chian School of Medicine, Nanyang Technological University, Singapore, 308232

GABA$_A$ receptors (GABA$_A$Rs) are profoundly important for controlling neuronal excitability. Spontaneous and familial mutations to these receptors feature prominently in excitability disorders and neurodevelopmental deficits following disruption to GABA-mediated inhibition. Recent genotyping of an individual with severe epilepsy and Williams-Beuren syndrome identified a frameshifting *de novo* variant in a major GABA$_A$R gene, *GABRA1*. This truncated the α1 subunit between the third and fourth transmembrane domains and introduced 24 new residues forming the mature protein, α1^{Lys374Serfs*25}. Cell surface expression of mutant murine GABA$_A$Rs is severely impaired compared with WT, due to retention in the endoplasmic reticulum. Mutant receptors were differentially coexpressed with β3, but not with β2, subunits in mammalian cells. Reduced surface expression was reflected by smaller IPSCs, which may underlie the induction of seizures. The mutant does not have a dominant-negative effect on native neuronal GABA$_A$R expression since GABA current density was unaffected in hippocampal neurons, although mutant receptors exhibited limited GABA sensitivity. To date, the underlying mechanism is unique for epileptogenic variants and involves differential β subunit expression of GABA$_A$R populations, which profoundly affected receptor function and synaptic inhibition.

Key words: α subunit variant; epilepsy; GABA-A receptor; inhibition; synaptic transmission

Significance Statement

GABA$_A$Rs are critical for controlling neural network excitability. They are ubiquitously distributed throughout the brain, and their dysfunction underlies many neurologic disorders, especially epilepsy. Here we report the characterization of an α1-GABA$_A$R variant that results in severe epilepsy. The underlying mechanism is structurally unusual, with the loss of part of the α1 subunit transmembrane domain and part-replacement with nonsense residues. This led to compromised and differential α1 subunit cell surface expression with β subunits resulting in severely reduced synaptic inhibition. Our study reveals that disease-inducing variants can affect GABA$_A$R structure, and consequently subunit assembly and cell surface expression, critically impacting on the efficacy of synaptic inhibition, a property that will orchestrate the extent and duration of neuronal excitability.

Received Nov. 18, 2019; revised May 5, 2020; accepted May 6, 2020.

Author contributions: S.H., D.N., and T.G.S. designed the research; S.H., A.H.B.A., M.M., C.J., P.G., B.P., G.W., and R.T. performed research; S.H., A.H.B.A., M.M., C.J., and T.G.S. analyzed data; S.H. and T.G.S. wrote the paper; All authors contributed to the writing of the paper.

T.G.S. and S.H. were supported by Medical Research Council United Kingdom, Wellcome Trust, and International Rett Syndrome Foundation (3606). D.N. was supported by Singapore National Medical Research Council NMRC/CIRG/1438/2015, Singapore Ministry of Education Academic Research Fund Tier 2 Grant 2015-T2-1-023, and Wellcome Trust "LonDownS Consortium" Strategic Funding Award 098330/Z/12/Z. B.P. was supported by the Deutsche Forschungsgemeinschaft Grant PO2366/2-1.

M. Minere's presentaddress: Max Planck Institute for Metabolism, Gleueler Strasse 50, Cologne, 50931, Germany.

C Jones's present address: Department of Pharmacology, University of Cambridge, Tennis Court Road, Cambridge, CB2 1PD, UK.

The authors declare no competing financial interests.

Correspondence should be addressed to Saad Hannan at s.hannan@ucl.ac.uk or Trevor G. Smart at t.smart@ucl.ac.uk.

https://doi.org/10.1523/JNEUROSCI.2748-19.2020

Introduction

γ-Aminobutyric acid (GABA) Type A receptors (GABA$_A$Rs) maintain homeostasis over brain excitation by mediating membrane hyperpolarization and shunting of neuronal excitability (Mitchell and Silver, 2003; Mann and Paulsen, 2007). GABA$_A$Rs are heteropentamers assembled from 19 subunits encoded by eight gene families: *GABRA1-6*, *GABRB1-3*, *GABRG1-3*, *GABRR1-3*, *GABRD*, *GABRE*, *GABRP*, and *GABRQ* (Sieghart and Sperk, 2002). The prototypical GABA$_A$R is composed of 2α, 2β and a γ or δ subunit, with those containing α1 being the most abundant subtype, particularly in the cortex where they account for the majority of synaptic GABA$_A$Rs (Hutcheon et al., 2004; Datta et al., 2015). Given their pivotal role in the brain, mutant GABA$_A$R subunits frequently underlie excitability

disorders, such as epilepsy (Macdonald et al., 2004; Maljevic et al., 2019).

Recently, an individual with dual pathology of Williams-Beuren syndrome (WBS) and severe epilepsy was identified (Popp et al., 2016). The neurologic phenotypes of WBS are characterized by cognitive and neurodevelopmental impairment, hypotonia, poor balance, and coordination (Popp et al., 2016). However, in addition to the WBS-associated microdeletion on chromosome 7, a *de novo* single-base deletion c.1200del, p.(Lys401Serfs*25, numbering includes the signal peptide) in the *GABRA1* gene was observed. This caused a frameshift that removed all residues from Lys374 onward to the C-terminus of the mature human protein while introducing 24 new amino acids followed by a stop codon ($\alpha1^{Lys374Serfs*25}$; referred to hereafter as $\alpha1^{Mut}$). Thus, the frameshift prematurely truncates the predominant $GABA_AR$ α subunit in the brain, removing part of the M3-M4 loop and the downstream fourth transmembrane (M4) domain and C-terminal.

Given the likely important consequences for inhibitory signaling following a drastic structural change to the $\alpha1$ subunit, including the insertion of new residues, we have characterized the molecular pharmacological properties of mutant $GABA_ARs$ in heterologous expression systems and neurons using electrophysiology, flow cytometry, and imaging. We identify severe impairments to cell surface $GABA_AR$ expression, reduced GABA sensitivity, and unexpected differential effects on receptor assembly.

Materials and Methods

Neurologic monitoring and EEG

As a result of the intractable epileptic encephalopathy, the individual carrying the variant c.1200del, p.(Lys401Serfs*25) in *GABRA1* was regularly seen at the pediatric neurology clinic (as an outpatient) in Erlangen. EEG monitoring was performed by an experienced pediatrician trained in neurophysiology and epileptology using standard investigative practice and established procedures. Informed written consent for publication of this clinical case was obtained from the legal guardians, and publication of the updated clinical course is covered by the ethical vote for retrospective translational research studies under the auspices of the Ethical Committee of the Medical Faculty of the Friedrich-Alexander-Universität Erlangen-Nürnberg.

cDNA and molecular biology

cDNAs for WT mouse $\alpha1$, $\beta2$, $\beta3$, $\beta3^{DNTK}$, $\gamma2L$, $\alpha1^{myc}$, and eGFP have been described previously (Taylor et al., 1999; Hannan and Smart, 2018; Hannan et al., 2020). Mouse $\alpha1^{Lys373Serfs*25}$ (equivalent to human $\alpha1^{Lys401Serfs*25}$ with signal sequence; $\alpha1^{Lys374Serfs*25}$ without signal sequence; defined hereafter as $\alpha1^{Mut}$) was created using $\alpha1$ as template and a single inverse PCR (Hannan et al., 2020) and ligation by removing 54 amino acids after Ser373 of the mature protein and adding 24 amino acids followed by a stop codon using CTAACAGTATCAGCAAAGTTA ACAGATTGTCAAGAATAGGTTCTTTTAGTCGTATTCTGTTG as forward and CGGCTTTCTAGGGTTTTGGTGATTTTGCTTTGGTGA GACTTCTTTCGGTTCTATGGTCGCAC as reverse primers. The $\alpha1^{\Delta373}$ subunit cDNA was created using inverse PCR with TAGGTT CTTTTAGTCGTATTCTGTTG as forward and CTTGACTTCTTT CGGTTCTATGGTCGC as reverse primers. The fidelity of all cDNAs was checked using DNA sequencing.

Cell culture

All cell culture reagents were acquired from Thermo Fisher Scientific unless otherwise stated. HEK-293T cells were grown at 37°C in 95% air/5% CO_2 in DMEM supplemented with 10% v/v FCS, penicillin-G/streptomycin (100 U/ml and 100 μg/ml) and 2 mM L-glutamine. Cells were seeded on 22 mm glass coverslips coated with poly-L-lysine (Sigma Millipore) for confocal imaging and whole-cell electrophysiology and in 6 cm adherent cell culture dishes for flow cytometry.

Primary hippocampal neurons

Use of animals conformed to the United Kingdom Animals (Scientific Procedures) Act 1986 and relevant European Union directives. Embryonic day 18 (E18) Sprague Dawley rat hippocampi of either sex were dissected in ice-cold HBSS, and dissociated neurons were seeded onto 18 mm glass coverslips coated with poly-D-lysine (Sigma Millipore) in a plating media containing MEM supplemented with 5% v/v FCS, 5% v/v horse serum, penicillin-G/streptomycin (100 U/ml and 100 μg/ml), 20 mM glucose (Sigma Millipore), and 2 mM L-glutamine. Two hours after seeding, the plating media was removed and replaced with a maintenance media comprising Neurobasal-A with 1% v/v B-27, penicillin-G/streptomycin (100 U/ml/100 μg/ml), 0.5% v/v Glutamax, and 35 mM glucose. Neurons were grown at 37°C and 95% air/5% CO_2.

Transfection

HEK-293 cells were transfected with cDNAs encoding for eGFP along with WT or mutant $\alpha1$ subunits, with $\beta2/3$ and $\gamma2L$ in equimolar ratios (1:1:1:1) using a calcium chloride method (Hannan and Smart, 2018). Neurons were transfected at 7 DIV with eGFP along with WT or mutant $\alpha1$ subunits in equimolar ratios also using a calcium chloride method (Hannan et al., 2013).

Oocytes and two electrode voltage clamp

Xenopus laevis ovaries were removed from frogs and incubated for 2-3 h in collagenase Type I (Worthington) in OR2 solution containing the following (in mM): 85 NaCl, 5 HEPES, and 1 $MgCl_2$, pH 7.6, adjusted with KOH. Defolliculated oocytes were washed in OR2 and maintained at 18°C in Barth's solution containing the following (in mM): 88 NaCl, 1 KCl, 0.33 $Ca(NO_3)_2$, 0.41 $CaCl_2$, 0.82 $MgSO_4$, 2.4 $NaHCO_3$, and 10 HEPES, pH adjusted to 7.6 with NaOH. Oocytes were injected with 27.6 nl of a 30 ng/µl mix containing WT or mutant $\alpha1$ subunits, $\beta2/3$ and $\gamma2L$ in equimolar ratios (1:1:1) and used for two-electrode voltage-clamp recordings 1-2 d after injection.

Two-electrode voltage clamp recordings were performed at room temperature in a recording solution containing the following (in mM): 100 NaCl, 2 KCl, 2 $CaCl_2$, 1 $MgCl_2$, and 5 HEPES, pH adjusted to 7.4 with NaOH, using an Axoclamp 2B amplifier, a Digidata 1322A interface, and pClamp 8 (Molecular Devices). Oocytes were voltage-clamped at −60 mV, and current data were digitized at 500 Hz and filtered at 50 Hz. GABA concentration-response curves were constructed as described in Electrophysiology.

Flow cytometry

Forty-eight hours after transfection, HEK-293 cells were washed with HBSS to remove growth media and incubated in trypsin for 30 s with gentle tapping to dislodge cells into suspension. The reaction was stopped with serum-containing HEK-293 growth media; and after centrifugation, the pellet containing the cells was resuspended in ice-cold PBS (Sigma Millipore) supplemented with 10% FCS and 1% sodium azide. From this point onward, all reactions were conducted in the serum containing PBS at 4°C. For labeling cell surface $GABA_ARs$, cells were centrifuged one more time before resuspension in a rabbit primary antibody against an N-terminal extracellular epitope of the $\alpha1$ subunit (Abcam Ab 33299) and incubated for 30-45 min under gentle shaking. Cells were washed twice to remove primary antibodies and then incubated in AlexaFluor-647-conjugated anti-rabbit secondary antibody for 30 min under gentle shaking. Cells were washed twice to remove secondary antibodies and immediately transported to the flow cytometry facility for data acquisition.

For measuring the amount of total receptors, cells were harvested and washed to remove media and fixed in 4% PFA in PBS for 10 min at room temperature under gentle shaking. Cells were washed twice in the serum-containing PBS to remove excess PFA and incubated in 0.1% Triton X in PBS for 10 min at room temperature under gentle shaking to permeabilize the membrane. After washing twice, cells were resuspended in a mouse primary antibody against $\alpha1$ subunits (NeuroMab clone

N95/35) and incubated for 30 min at 4°C under gentle shaking. Cells were washed twice to remove primary antibodies and incubated in AlexaFluor-647-conjugated anti-mouse secondary antibody for 30 min at 4°C under gentle shaking. Cells were washed twice to remove secondary antibodies before flow cytometry.

Flow cytometry was conducted using a BD FACS Aria IIIu fitted with blue (488 nm), red (633 nm), violet (405 nm), and yellow-green (561 nm) lasers and FACS Diva software version 8.0.1. Cells were gated on forward scatter versus side scatter and cell doublets discriminated by side scatter-W parameter. GFP and AlexaFluor-647 were detected on the blue laser 530/30 nm and red laser 660/20 nm parameters using area.

Based on the auto-fluorescence profiles of untreated or primary and secondary antibody-incubated untransfected cells, the levels of background fluorescence were segmented in fluorescence scatter plots of eGFP against AlexaFluor-647 expression levels of cells. This gave rise to four quadrants: Q1, AlexaFluor-647 only; Q2, eGFP and AlexaFluor-647; Q3, autofluorescence; and Q4, eGFP only. The median cell surface fluorescence intensity for mutant GABA$_A$Rs in Q2 was normalized to the corresponding median for WT GABA$_A$Rs in the same run. In addition, the median %Q2 area or the % of cells in Q2, which is representative of the efficiency of cell surface expression, was normalized to the median %Q2 area for WT GABA$_A$Rs.

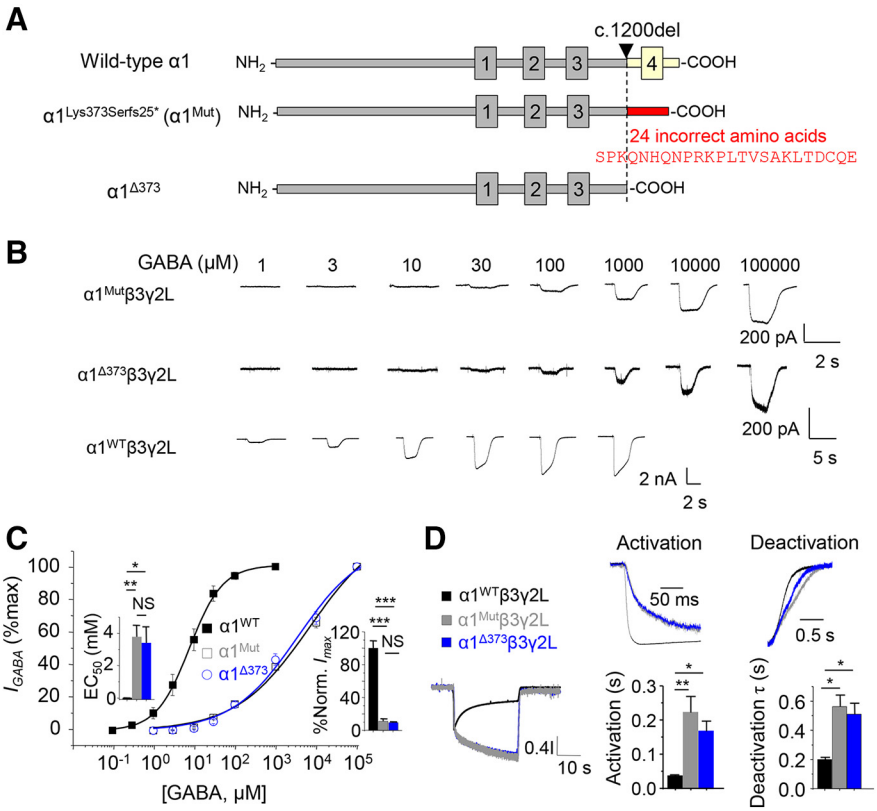

Figure 1. Severe reduction in the GABA sensitivity of mutant α1-GABA$_A$Rs. ***A***, Schematic showing the location of the α1-GABA$_A$R variant in the M3-M4 loop with and without the additional 24 amino acids. ***B***, GABA-activated currents for WT and mutant α1 subunits expressed with β3γ2L in HEK-293 cells. ***C***, GABA concentration-response relationships for WT and α1 mutant receptors. Insets, GABA EC$_{50}$s and normalized maximal GABA currents. ***D***, Averaged currents evoked by saturating GABA (1 mM WT, 100 mM mutants). Examples of activation and deactivation of GABA currents are shown together with averaged activation and deactivation rates. Activation rate was calculated by measuring the time taken to ascend from 20% to 80% of maximal current following the application of GABA. Deactivation rate was calculated by exponential fitting to the current decay immediately after cessation of GABA application. NS, not significant; *$p < 0.05$; **$p < 0.01$; ***$p < 0.001$; one-way ANOVA.

Immunolabeling and confocal imaging

HEK-293 cells and neurons were washed with PBS and fixed in 4% PFA for 10 min at room temperature followed by incubation in primary antibody (mouse anti-myc; Abcam, Ab32) in PBS containing 3% FCS at room temperature for 45 min. After washes to remove the primary antibody, cells were incubated in secondary antibody (goat anti-mouse AlexaFluor-555) in PBS containing 3% FCS at room temperature for 30 min. After serial washing, cells were mounted in the antifade agent, ProLong gold.

For permeabilized cells, after fixation, incubation proceeded in 0.1% Triton X in PBS containing 10% FCS for 10 min at room temperature followed by serial washes and incubation in primary (mouse anti-α1, Neuromab; rabbit anti-calnexin, Ab22595) and secondary (goat anti-mouse AlexaFluor-555; goat anti-rabbit 647) antibodies. Cells were mounted in ProLong gold reagent.

Confocal imaging was undertaken using an LSM 510 Meta microscope with a 40× oil-immersion objective and a 488 nm laser for imaging eGFP, 543 nm laser for imaging AlexaFluor-555, and 634 nm laser for imaging AlexaFluor-647. Cells were imaged sequentially at optimum optical thickness in 8-bit.

Image analysis

Images were analyzed using ImageJ (version 1.52i). Mean cell surface fluorescence levels were measured from defined ROIs around the periphery of cells (Hannan et al., 2013). Colocalization analysis was undertaken using Just Another Co-localization Plugin (JACoP) in ImageJ. After applying thresholds, Pearson's coefficient (r) between α1 subunit and ER fluorescence values for individual pixels was determined. In addition, the proportion of α1 subunit fluorescence that colocalized with the ER (Manders coefficient M1) and the proportion of ER fluorescence that colocalized with α1 subunits (Mander's coefficient M2) were also measured.

Electrophysiology

Whole-cell electrophysiology of HEK-293 cells was conducted 48 h after transfection by voltage clamping cells at −30 mV with optimized series resistance (R_s, <10 MΩ) and whole-cell membrane capacitance compensation. Borosilicate glass patch electrodes (resistances of 3-5 MΩ) were filled with an internal solution containing (mM) as follows: 120 CsCl, 1 $MgCl_2$, 11 EGTA, 30 KOH, 10 HEPES, 1 $CaCl_2$, and 2 K_2ATP, pH 7.2. Cells were superfused with a saline solution containing (in mM) as follows: 140 NaCl, 4.7 KCl, 1.2 $MgCl_2$, 2.52 $CaCl_2$, 11 glucose, and 5 HEPES, pH 7.4. Membrane currents were filtered at 5 kHz (−3 dB, sixth pole Bessel, 36 dB per octave).

GABA concentration-response curves were constructed by measuring GABA-activated currents (I) elicited at each GABA concentration and normalizing these currents to maximal responses (I_{max}). The concentration-response relationship was fitted with the Hill equation as follows:

$$I/I_{max} = (1/\left(1 + (EC_{50}/[A])^n\right)$$

where A is the concentration of GABA, EC_{50} is the concentration of GABA giving 50% of the maximum response, and n is the Hill slope.

The kinetics of GABA-activated currents in HEK-293 cells was studied by applying 1 mM GABA (for WT receptors) and 100 mM GABA (for

Table 1. Mean EC_{50}s, maximal GABA-activated currents, activation, and deactivation rates for GABA currents mediated by mutant and WT α1 subunit receptors expressed in HEK-293 cells with β and γ2L subunits

	EC_{50}	SEM	Units	*N* (cells)	*N* (trials)	Average Hill slope	Figure
HEK cells							
$\alpha1\beta3\gamma2L$	8.8	1.7	μm	6	3	1.2 ± 0.1	1*C*
$\alpha1^{Lys373Serfs*25}\beta3\gamma2L$	3798	704	μm	7	3	0.6 ± 0.03	
$\alpha1^{\Delta373}\beta3\gamma2L$	3406	999	μm	6	2	0.6 ± 0.04	
	I Max						
$\alpha1\beta3\gamma2L$	100	—		11	3		1*C*
$\alpha1^{Lys373Serfs*25}\beta3\gamma2L$	11.1	2.9	% control	7	3		
$\alpha1^{\Delta373}\beta3\gamma2L$	9.4	1	% control	8	3		
	Activation rate						
$\alpha1\beta3\gamma2L$	0.036	0.004	s	8	2		1*D*
$\alpha1^{Lys373Serfs*25}\beta3\gamma2L$	0.22	0.05	s	9	2		
$\alpha1^{\Delta373}\beta3\gamma2L$	0.17	0.03	s	7	2		
	Deactivation τ						
$\alpha1\beta3\gamma2L$	0.2	0.02	τ (s)	5	2		1*D*
$\alpha1^{Lys373Serfs*25}\beta3\gamma2L$	0.56	0.08	τ (s)	10	2		
$\alpha1^{\Delta373}\beta3\gamma2L$	0.51	0.08	τ (s)	9	2		

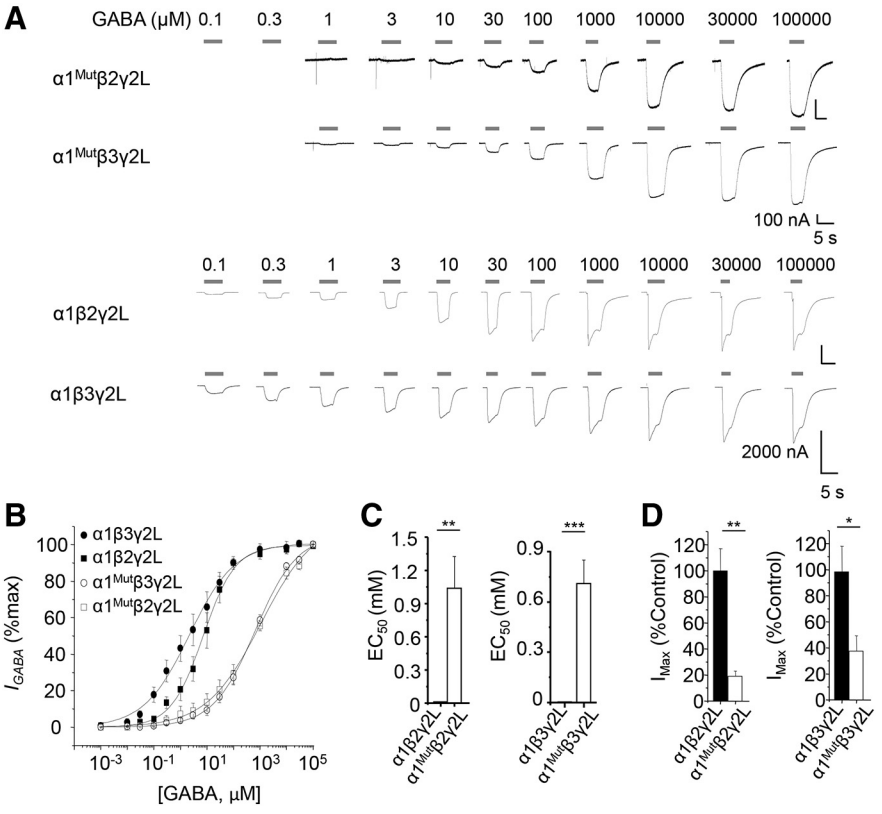

Figure 2. Reduced sensitivity to GABA for α1 mutants expressed in *Xenopus* oocytes. ***A***, Representative GABA-activated currents for WT and mutant receptors expressed in *Xenopus* oocytes with $\beta2\gamma2L$ or $\beta3\gamma2L$. ***B***, GABA concentration-response relationships for WT and α1 mutant receptors. ***C***, GABA EC_{50}s for $\alpha1\beta2\gamma2L$ ($n=7$); $\alpha1^{Mut}\beta2\gamma2L$ ($n=5$); $\alpha1\beta3\gamma2L$ ($n=8$); and $\alpha1^{Mut}\beta3\gamma2L$ ($n=5$). ***D***, Maximum GABA-activated currents for WT and mutant α1 receptors. The maximal GABA concentration applied was 100 mM. Normalized maximal currents (to WT) shown for $\alpha1\beta2\gamma2L$ ($n=7$); $\alpha1^{Mut}\beta2\gamma2L$ ($n=8$); $\alpha1\beta3\gamma2L$ ($n=7$); and $\alpha1^{Mut}\beta3\gamma2L$ ($n=5$). *$p<0.05$; **$p<0.01$; ***$p<0.001$; two-tailed unpaired *t* test.

mutant receptors) via a modified U-tube (Thomas and Smart, 2012). The activation rate was estimated by measuring the time taken to ascend 20%–80% of I_{max} during GABA application. The deactivation rate was estimated by fitting a single exponential function from the point when GABA application ceased until the baseline was reached.

Neurons transfected at 7 DIV with WT or mutant α1 subunit cDNAs were voltage clamped at –60 mV for recording GABA-activated currents or sIPSCs at 12-14 DIV. Neurons were superfused with the same saline solution as used for HEK-293 cells but containing 2 mM kynurenic acid to block excitatory neurotransmission. Membrane capacitance was measured by applying brief −10 mV pulses to hyperpolarize the membrane and calculating the area under the capacity current discharge curve. Current densities were measured by dividing maximal GABA currents obtained with 1 mM GABA at −20 mV holding potential with the membrane capacitance. Cumulative probability distributions of sIPSC amplitudes and areas mediated by WT and mutant receptors were compared using nonparametric statistics, whereas mean sIPSC frequency, T_{50}, and decay τ were compared by using parametric tests.

Modeling GABA concentration-response curves

To predict the GABA concentration-response curves for a varying mixture of subpopulations of $GABA_ARs$ containing either only $\alpha1^{WT}$ or $\alpha1^{Mut}$ subunits, or a binomial mixture of both, with $\beta3$ and $\gamma2L$ subunits, we devised the following modified Hill equation:

$$I_{GABA} = \left[\frac{[A]}{[A]+EC_{50}1}\right]^{i} u * n + \left[\frac{[A]}{[A]+EC_{50}2}\right]^{j} v * m + \left[\frac{[A]}{[A]+EC_{50}3}\right]^{k} w * p$$

Where the GABA current (I_{GABA}) compared with the maximal response for each GABA concentration ($[A]$) is determined by up to three populations of $GABA_ARs$ expressed with relative proportions of n, m, and p (where $m+n+p=1$) and trafficking factors u, v, and w, where a value of 1 signifies efficient near-complete expression at the cell surface and 0 no surface expression. $EC_{50}1$, $EC_{50}2$, and $EC_{50}3$ represent the concentrations of GABA evoking 50% of the maximal GABA response for $\alpha1^{WT}$, $\alpha1^{WT}+$

$\alpha1^{Mut}$, and $\alpha1^{Mut}$, respectively. *i*, *j*, and *k* represent the Hill slope factors. For single populations of $GABA_A$Rs, the conventional Hill equation was used to provide curve fits to the GABA concentration-response data as follows:

$$I_{GABA} = \left[\frac{[A]^i}{[A]^i + EC50^i}\right]$$

where the symbols are as previously defined.

Nonstationary noise analysis

For peak-scaled nonstationary variance analysis, synaptic GABA currents were individually selected for clean rise and decay phases (i.e., lacking inflections, secondary peaks, or current artifacts). The clean synaptic currents were imported into WinWCP version 5.2.3 (John Dempster, University of Strathclyde, Glasgow), and the peak of the averaged sIPSCs was aligned to the negative rise phase and peaks of the individual sIPSCs chosen for the analysis. The decay phases of individual sIPSCs were subtracted from the mean sIPSC decay to generate the sIPSC variance, which was plotted against the corresponding mean current according to the parabolic function as follows:

$$\sigma^2 = [\mathrm{i.I_{m-}}(\mathrm{I_m^2/N})] + \mathrm{Var_b}$$

Where σ^2 is the current variance, *i* represents single-channel current, I_m is the mean current and *N* is the average number of synaptic receptors activated during the peak of an sIPSC. Var_b represents the baseline current variance. This equation was used to generate fits to the current variance – mean plots and to estimate *i* and *N* for synaptic $GABA_A$Rs.

Experimental design and statistics

All statistical tests that have been used, and applied to sample sizes in the study, are indicated in the figure legends and in Results. For parametric data, two groups were compared using two-tailed Student's *t* test. For comparing data from three or more groups, a one-way ANOVA was used (GraphPad Instat 3). Where normality in the data spread was not apparent, we used nonparametric tests in conjunction with SPSS (version 24). Data in the bar charts represent mean ± SEM. Data in box plots show 25%-75% interquartile ranges and the median.

Results

Severe epileptic encephalopathy with mutant $GABA_A$Rs

The patient's clinical characteristics up to the age of 14 months have been reported previously when the variant c.1200del, p.(Lys401Serfs*25) in *GABRA1* and the common microdeletion in 7q11.23 were identified as the genetic cause of the phenotype, including refractory epileptic encephalopathy and characteristic features of WBS (Popp et al., 2016). Since that period, the patient's anticonvulsant therapy has been regularly optimized. Repeated EEG analyses confirmed severe epileptic encephalopathy with slow background activity and diffuse epileptic discharges. At age 38 months, epileptic episodes were characterized by daily myoclonic seizures and rare short-tonic seizures lasting 30–60 s. Global neurodevelopmental deficits, including hypotonic-ataxic cerebral palsy and severe intellectual disability, were also evident.

The physiological consequences of the genetic variation were probed by generating an equivalent mouse $\alpha1$ subunit replicating the truncation in the human subunit starting from lysine 373 of the mature $\alpha1$ protein (equivalent to human Lys374), followed by the addition of 24 *de novo* residues that are found in the WBS individual (designated as $\alpha1^{Mut}$; Fig. 1*A*). In addition, a truncation mutant from Lys373 that excluded the frameshift was also created to examine the effect of the 24 additional new residues (designated as $\alpha1^{\Delta373}$; Fig. 1*A*) on $GABA_A$R function.

Table 2. Mean cell surface fluorescence and % area Q2 of flow cytometry

	Mean normalized	SEM	*N* (trials)	Figure
Median surface fluorescence				
$\alpha1\beta2\gamma2L$	100	—	7	3*B*
$\alpha1^{Lys373Serfs*25}\beta2\gamma2L$	60.9	9.5	7	
$\alpha1^{\Delta373}\beta2\gamma2L$	47.7	7.2	5	
Untransfected	0	0	7	
eGFP control	0	0	7	
Median surface fluorescence				
$\alpha1\beta3\gamma2L$	100	—	6	3*C*
$\alpha1^{Lys373Serfs*25}\beta3\gamma2L$	29.2	6.3	6	
$\alpha1^{\Delta373}\beta3\gamma2L$	32.1	6.7	5	
Untransfected	0	0	6	
eGFP control	0	0	6	
Median intracellular fluorescence				
$\alpha1\beta2\gamma2L$	100	—	5	3*E*
$\alpha1^{Lys373Serfs*25}\beta2\gamma2L$	86.3	6.7	5	
Untransfected	0	0	5	
eGFP control	0	0	5	
$\alpha1\beta3\gamma2L$	100	—	5	3*F*
$\alpha1^{Lys373Serfs*25}\beta3\gamma2L$	89.2	8.4	5	
Untransfected	0	0	5	
eGFP control	0	0	5	
Surface Q2 area				
$\alpha1\beta2\gamma2L$	100	—	7	3*B*
$\alpha1^{Lys373Serfs*25}\beta2\gamma2L$	6.1	1.6	7	
$\alpha1^{\Delta373}\beta2\gamma2L$	5.2	1.1	5	
Untransfected	0	0	7	
eGFP control	0	0	7	
$\alpha1\beta3\gamma2L$	100	—	6	3*C*
$\alpha1^{Lys373Serfs*25}\beta3\gamma2L$	24.7	4.3	6	
$\alpha1^{\Delta373}\beta3\gamma2L$	39.8	3.2	5	
Untransfected	0	0	6	
eGFP control	0	0	6	
Intracellular Q2 area				
$\alpha1\beta2\gamma2L$	100	—	5	3*E*
$\alpha1^{Lys373Serfs*25}\beta2\gamma2L$	84.1	14.5	5	
Untransfected	0	3.2	5	
eGFP control	0	0	5	
$\alpha1\beta3\gamma2L$	100	—	5	3*F*
$\alpha1^{Lys373Serfs*25}\beta3\gamma2L$	121	27	5	
Untransfected	0	0	5	
eGFP control	0	0	5	
Surface Q2 area				
$\alpha1\beta3\gamma2L$	100	—	3	4*B*
$\alpha1^{Lys373Serfs*25}\beta3\gamma2L$	33.1	3	3	
$\alpha1^{Lys373Serfs*25}\beta3^{DNTK}\gamma2L$	19.9	4.2	3	
Untransfected	0.1	0.03	3	
eGFP control	0	0	3	

A majority of $\alpha1$-$GABA_A$Rs are coassembled with $\beta2/\beta3$ and $\gamma2L$ subunits in the brain (Whiting, 2003). Thus, GABA sensitivity of $\alpha1^{Mut}$ was studied in isolation in HEK-293 cells coexpressed with either $\beta2$ or $\beta3$ subunits and $\gamma2L$. Receptors comprising $\alpha1^{Mut}\beta3\gamma2L$ and $\alpha1^{\Delta373}\beta3\gamma2L$ receptors were considerably less sensitive to GABA ($F_{(2,16)} = 8.491$, $p = 0.0031$, one-way ANOVA, Table 1; Fig. 1*B*,*C*) and with lower maximal currents ($F_{(2,23)} = 61.823$, $p < 0.001$, one-way ANOVA; Fig. 1*B*, *C*). There was no difference ($p = 0.918$ and $p = 0.986$, respectively, Tukey-Kramer *post hoc* test) between the two mutants, suggesting that the additional 24 amino acids do not additionally affect GABA potency and/or receptor activation. Of note, both mutant receptors failed to activate in response to 100 mM GABA when assembled with $\beta2$ subunits ($\alpha1^{Mut}\beta2\gamma2L$ and $\alpha1^{\Delta373}\beta2\gamma2L$), highlighting the importance of the β subunit for assembly,

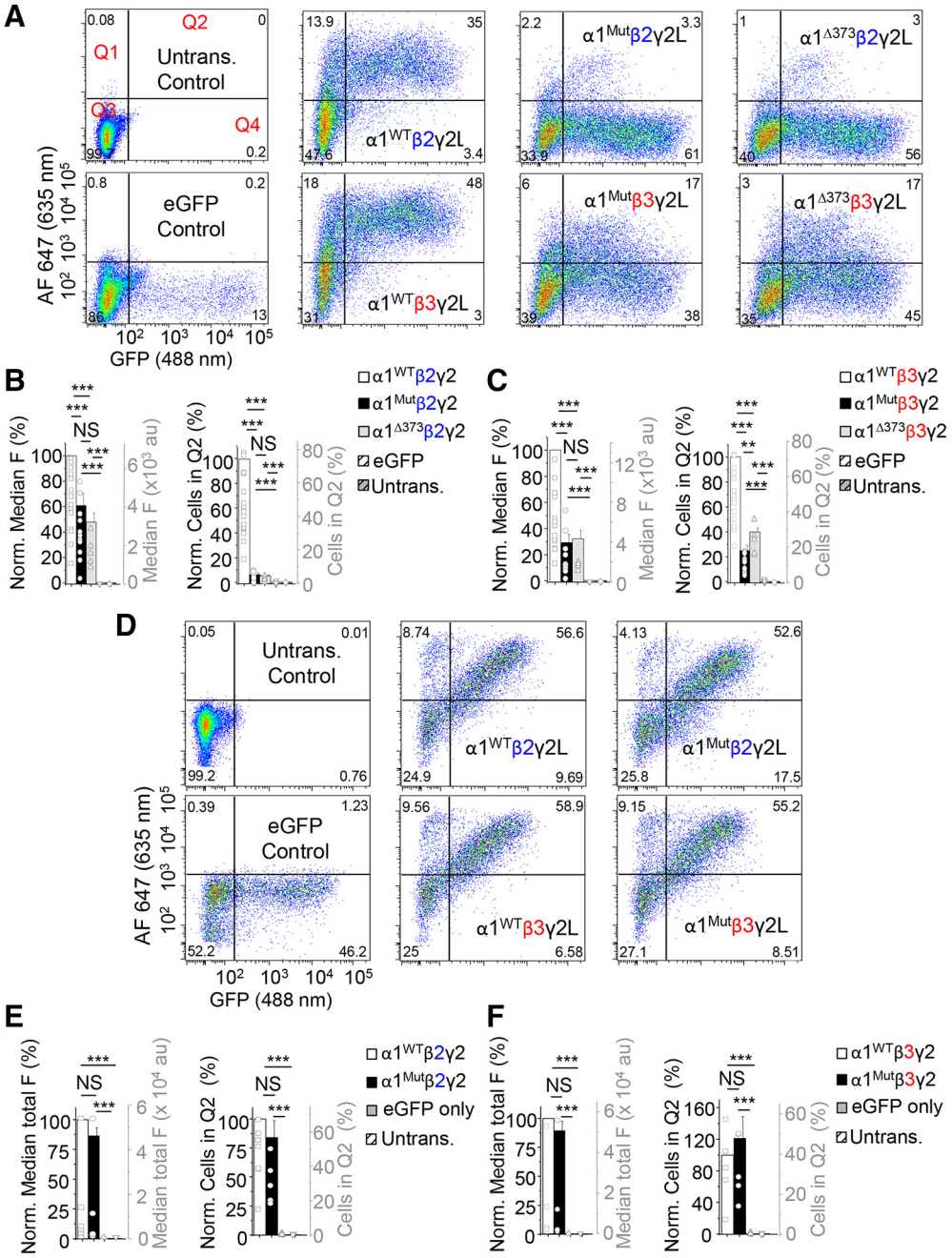

Figure 3. Impaired cell surface expression of $\alpha 1$ mutant GABA$_A$Rs in HEK-293 cells. ***A***, Cytofluorograms for cell surface $\alpha 1$ WT and mutant GABA$_A$Rs in HEK-293 cells expressed with either $\beta 2\gamma 2$L (top line) or $\beta 3\gamma 2$L (bottom) subunits. The numbers in quadrants (Q1-Q4) show percentages of detected cells. ***B***, ***C***, Left, Normalized (Norm.; %) median cell surface fluorescence (***F***) for: ***B***, $\alpha 1^x\beta 2\gamma 2$L and ***C***, $\alpha 1^x\beta 3\gamma 2$L (where x = WT, Mut or Δ373), including eGFP and untransfected (untrans.) controls in Q2. Right, Mean % number of expressing cells in Q2 for $\alpha 1^x\beta 2\gamma 2$L (***B***) and $\alpha 1^x\beta 3\gamma 2$L (***C***). Non-normalized data points are shown by symbols superimposed on the bar charts with the right-hand ordinate denoting their values. au, Arbitrary units. ***D***, Cytofluorograms for total (intracellular and surface) $\alpha 1$ WT and mutant receptors in permeabilized HEK-293 cells expressing $\beta 2\gamma 2$L or $\beta 3\gamma 2$L. ***E***, ***F***, Left, Median (%) total fluorescence for $\alpha 1^x\beta 2\gamma 2$L (***E***) and $\alpha 1^x\beta 3\gamma 2$L (***F***). Right, % cells in Q2 expressing $\alpha 1^x\beta 2\gamma 2$L (***E***) and $\alpha 1^x\beta 3\gamma 2$L (***F***). All data are normalized to the WT data. NS, not significant; $^{**}p < 0.01$; $^{***}p < 0.001$; one-way ANOVA. $n = 5$-7 independent experiments with 25,000-50,000 cells per construct per run.

trafficking, and/or signaling of $\alpha 1^{Mut}$-containing heteromers in mammalian cells.

Receptor activation, desensitization, and deactivation of recombinant $\alpha 1^{Mut}\beta 3\gamma 2$L and $\alpha 1^{\Delta 373}\beta 3\gamma 2$L were studied by applying maximal GABA concentrations (1 mM for WT and 100 mM for each mutant). Both mutant receptors displayed slower activation ($p = 0.0025$) and deactivation ($p = 0.0171$) kinetics compared with WT receptors (Fig. 1*D*), suggesting a profound defect(s) in gating and/or GABA binding. Moreover, neither mutant showed evidence of macroscopic desensitization (Fig. 1*D*). These results indicated that adding 24 new amino acids to the $\alpha 1$ subunit did not alter the signaling properties of mutant receptors compared with the truncated form of the receptor.

To further assess the differential expression profile of $\alpha 1^{Mut}$ with $\beta 2$ and $\beta 3$ subunits, we reverted to an amphibian expression system that permits the expression of a wider range of constructs compared with mammalian cells (Hanrahan, 2004) and also enables longer cell incubation times to resolve slower rates of receptor expression (Smart and Krishek, 1995),

which may be missed in HEK cells. As noted with HEK-293 cell expression, both the sensitivity to GABA ($p < 0.001$; Fig. 2*A–C*) and maximal GABA current ($p = 0.0382$; Fig. 2*A,D*) for $\alpha1^{Mut}\beta3\gamma2L$ were reduced compared with WT receptors when expressed in *Xenopus* oocytes. However, in contrast to HEK cells, $\alpha1^{Mut}\beta2\gamma2L$ were also expressed in oocytes to a similar extent to $\beta3$-containing receptors. GABA sensitivity ($p = 0.0015$) was reduced together with lowered maximal currents ($p = 0.0003$; Fig. 2*A-D*). These results confirmed the impaired GABA activation, gating, and GABA sensitivity of the mutant receptors and provided the first evidence that their expression and signaling properties depended on coassembly and/or trafficking with different β subunits in mammalian cells.

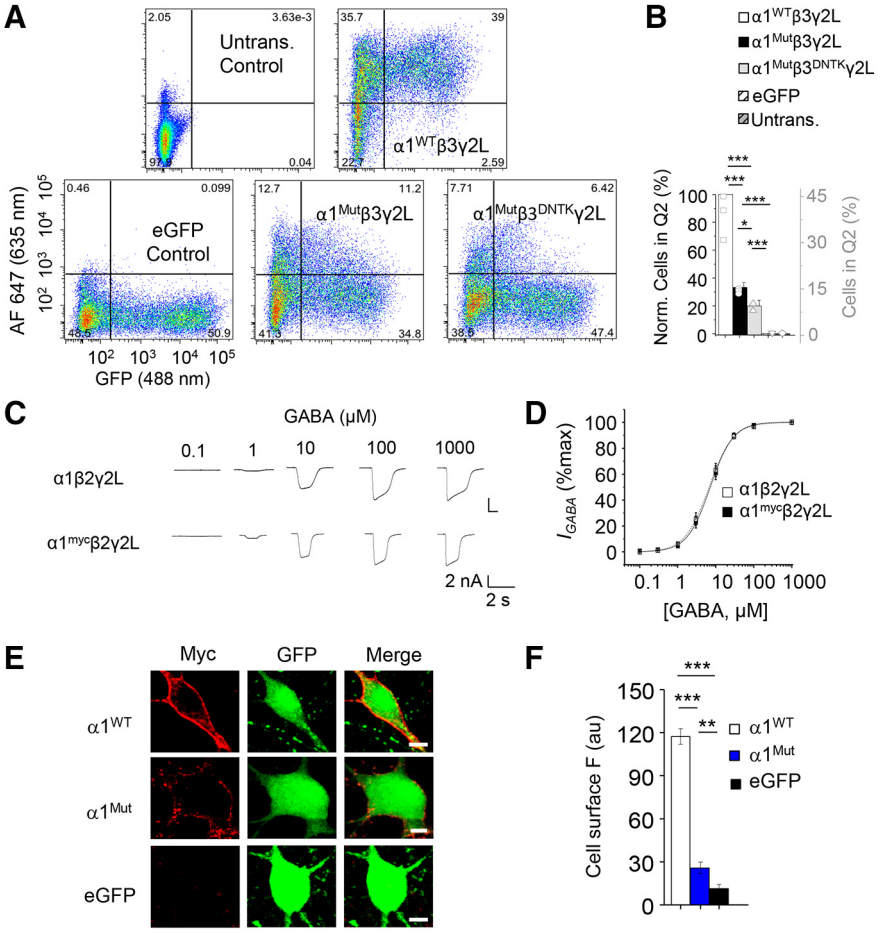

Figure 4. Effect of an assembly box sequence on cell surface expression and expression of $\alpha1$-GABA$_A$Rs in hippocampal neurons. ***A***, Cytofluorograms for cell surface $\alpha1$ WT and mutant GABA$_A$Rs in HEK-293 cells expressed with either $\beta3\gamma2L$ or $\beta3^{DNTK}\gamma2L$ subunits. ***B***, Normalized (Norm.) mean % number of expressing cells in Q2 for $\alpha1$ with $\beta3\gamma2L$ or $\beta3^{DNTK}\gamma2L$. Non-normalized data points are shown (symbols) on each bar chart with values denoted by the right-hand ordinate. *$p < 0.05$; ***$p < 0.001$; one-way ANOVA. $n = 3$ independent experiments with 25,000-50,000 cells per construct per run. ***C***, Representative GABA-activated currents for untagged and myc-tagged WT $\alpha1$ subunit receptors expressed in HEK-293 cells with $\beta2\gamma2L$ subunits to check functional neutrality of the myc-tag. ***D***, GABA concentration-response relationships for untagged or myc-tagged WT $\alpha1\beta2\gamma2L$ receptors. EC_{50s}, $\alpha1\beta2\gamma2L$, 7.2 ± 1 μM, $n = 8$; $\alpha1^{myc}\beta2\gamma2L$, 7.5 ± 1.2 μM, $n = 6$. ***E***, Confocal images of hippocampal cell surface labeling showing myc-tagged WT or mutant $\alpha1$-containing GABA$_A$Rs (left column), eGFP staining (middle), and merged images of $\alpha1$ and GFP fluorescence (right). Scale bars, 5 μm. ***F***, Mean fluorescence intensities for WT and mutant $\alpha1$-containing GABA$_A$R cell surface labeling in neurons. au, Arbitrary units. **$p < 0.01$; ***$p < 0.001$; one-way ANOVA. $n = 36$.

Impaired cell surface expression of mutant α1-GABA$_A$Rs

Reduced GABA-activated currents for mutant receptors and the absence of current for $\beta2$-containing mutant receptors in mammalian cells could reflect reduced cell surface expression. We studied this aspect using live HEK-293 cells expressing $\alpha1^{WT}$, $\alpha1^{Mut}$, or $\alpha1^{\Delta373}$ alongside $\beta2$ or $\beta3$, and $\gamma2L$ subunits. Surface expression was determined by flow cytometry in conjunction with an N-terminal $\alpha1$ subunit antibody. With $\beta2$ and $\gamma2L$ subunits, a substantive decrease in surface expression (>94%-95%; $F_{(4,28)} = 74.010$, $p < 0.001$, one-way ANOVA) was evident for $\alpha1^{Mut}$ and $\alpha1^{\Delta373}$, compared with $\alpha1^{WT}$ and eGFP controls (Table 2; Fig. 3*A,B*). Similarly, $\alpha1$ mutant or truncated receptors also exhibited reduced ($F_{(4,24)} = 115.331$, $p < 0.001$, one-way ANOVA) cell surface expression when coassembled with $\beta3$ and $\gamma2L$ (Fig. 3*A,C*). Although fivefold more receptors reached the cell surface with $\beta3$ compared with $\beta2$ subunits, surface expression was still severely impaired compared with WT controls ($F_{(4,24)} = 314.885$, $p < 0.001$, one-way ANOVA; Fig. 3*A,C*). Interestingly, the efficiency of expression was lower ($p = 0.02$, Tukey-Kramer *post hoc* test) for $\alpha1^{Mut}\beta3\gamma2L$ compared with $\alpha1^{\Delta373}\beta3\gamma2L$, suggesting that the additional 24 new amino acids affected subunit assembly and/or cell surface trafficking, a feature that was not apparent for $\beta2$-containing mutant receptors.

To discount the possibility that variable total receptor levels affected cell surface expression, flow cytometry was used to measure total (intracellular and surface) subunit levels in permeabilized cells expressing mutant and WT $\alpha1$ subunits, with either $\beta2$ ($F_{(3,16)} = 255.156$ (fluorescence)/54.140 (efficiency), $p < 0.001$, one-way ANOVA) or $\beta3$ subunits ($F_{(3,16)} = 166.694$ (fluorescence)/21.825 (efficiency), $p < 0.001$, one-way ANOVA), and $\gamma2L$ subunits. No differences ($p > 0.05$, Tukey-Kramer *post hoc*) in fluorescence intensities or expression efficiencies were observed between WT and mutant receptors (Fig. 3*D-F*), suggesting impaired cell surface expression of mutant receptors does not reflect intracellular expression levels.

To corroborate the flow cytometry results, we used immunocytochemistry and confocal imaging of GABA$_A$Rs expressed in HEK-293 cells by targeting the $\gamma2L$ subunit with an N-terminal antibody. This also revealed reduced surface expression of $\alpha1^{Mut}$ with $\beta3\gamma2L$-containing receptors and a near-complete loss of surface labeling for $\alpha1^{Mut}$ with $\beta2\gamma2L$-containing receptors (data not shown). Overall, these results demonstrate a severe reduction of cell surface expression of $\alpha1^{Mut}$-containing receptors that depends on the coassembled β subunit with only $\beta3$ supporting a severely limited surface expression of mutant GABA$_A$Rs in HEK-293 cells.

To explore which unique motifs in the $\beta3$ subunit enable coassembly with mutant $\alpha1$ subunits, we selected a conserved stretch of amino acids in the extracellular domain (ECD) previously shown to affect homomeric β subunit assembly.

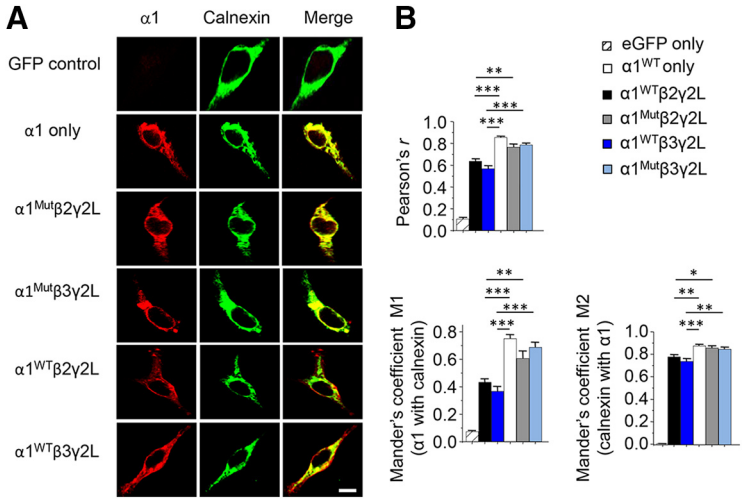

Figure 5. Intracellular retention of mutant GABA$_A$Rs in the ER. ***A***, Representative confocal images of WT and mutant α1-containing GABA$_A$Rs expressed in HEK-293 cells. Left column (from the top), Rows for cells expressing the following: GFP or α1 subunits only; $\alpha1^{Mut}$ with either β2 or β3 and γ2L; and $\alpha1^{WT}$ with either β2 or β3 and γ2L subunits. Middle column, Immunostains for the ER-associated protein, calnexin. Right column, The extent of colocalization for $\alpha1^{WT}$ and $\alpha1^{Mut}$ subunits with calnexin. The images are represented as pseudo-colors. ***B***, Bar graphs represent Pearson's correlation coefficient (*r*), and Mander's M1/2 coefficients also measuring colocalization of α1 and calnexin. M1 reports α1 colocalized with calnexin, and M2 denotes calnexin colocalized with α1 subunits. *$p < 0.05$; **$p < 0.01$; ***$p < 0.001$; one-way ANOVA. n = 18-28. Scale bar, 5 µm.

Substitution of the β3 GKER assembly box sequence to DNTK, found in β2 subunits (Taylor et al., 1999), reduced ($F_{(4,10)}$ = 316.991, $p < 0.001$, one-way ANOVA; p = 0.016, Tukey-Kramer *post hoc* test compared with $\alpha1^{Mut}$; Fig. 4*A*,*B*) but did not abolish cell surface expression of β3 subunits ($p = 0.001$ compared with eGFP controls; Fig. 4*A*,*B*). This suggests that the GKER motif in conjunction with other domains, including the TMDs and intracellular linkers, are important for the differential cell surface expression of $\alpha1^{Mut}$ with β3 subunits.

The effect of the frameshift on α1-GABA$_A$R cell surface levels was also studied in hippocampal neurons expressing either N-terminal myc-tagged $\alpha1^{WT}$ or $\alpha1^{Mut}$ subunits, and using coassembly with native β and γ2L subunits. The myc-tag did not affect α1 subunit receptor sensitivity to GABA ($p = 0.8303$; Fig. 4*C*,*D*). Immunolabelling with anti-myc antibodies in nonpermeabilized neurons revealed clear cell surface staining for myc-tagged $\alpha1^{WT}$ subunits. However, expression of myc-tagged $\alpha1^{Mut}$ was significantly compromised ($p < 0.001$, one-way ANOVA) but higher than background eGFP-only fluorescence levels ($p < 0.01$, one-way ANOVA) (Fig. 4*E*,*F*). Thus, impaired cell surface expression of mutant α1-GABA$_A$Rs was also apparent in hippocampal neurons.

Intracellular retention of mutant α1 subunits

To investigate whether mutant receptors were retained intracellularly, their colocalization with the ER marker calnexin (Leach and Williams, 2011) was studied in HEK-293 cells. As expected, WT α1 subunits were retained in the ER when expressed alone (Connolly et al., 1996). High colocalization between the α1 fluorophore and ER marker was signified by Pearson's regression (*r*) coefficient, and by Mander's M1 (fraction of α1 that colocalizes with calnexin) and M2 coefficients (fraction of calnexin that colocalizes with α1) (Fig. 5*A*,*B*). By contrast, WT receptors, expressed with β2/3γ2L, had lower Pearson's r ($F_{(5, 118)}$ = 120.349, $p < 0.001$, one-way ANOVA), Mander's M1 ($F_{(5, 117)}$ = 46.992, $p < 0.001$), and M2 ($F_{(5, 120)}$ = 244.694, $p < 0.001$) compared with α1 alone since WT heteromers exited the ER and were expressed at the cell surface.

For $\alpha1^{Mut}\beta$2/3γ2L receptors, increased ER retention was evident from the high Pearson's *r* and Mander's M1, M2 coefficients. These were near-identical to values determined for α1 alone ($p = 0.061$ to $p = 0.990$ Tukey-Kramer *post hoc* test) and significantly higher than those for WT $\alpha1\beta$2/3γ2L receptors ($p = 0.048$ to $p < 0.001$, Tukey-Kramer *post hoc* test; Fig. 5*A*,*B*). Thus, ER retention of $\alpha1^{Mut}$ impairs the cell surface expression of GABA$_A$Rs.

Epilepsy-inducing α1^{Mut} impairs GABAergic neurotransmission

To investigate the effect of $\alpha1^{Mut}$ on inhibitory transmission, we expressed $\alpha1^{WT}$ or $\alpha1^{Mut}$ subunits in hippocampal neurons at 7 DIV and studied sIPSCs at 12-16 DIV. For $\alpha1^{Mut}$-expressing neurons, sIPSC amplitudes were reduced (median $\alpha1^{WT}$, −63.4 pA, n = 5664 events from 24 cells; median $\alpha1^{Mut}$, −46.5 pA, n = 5236 events from 25 cells; $p < 0.001$, Mann–Whitney test; Fig. 6*A*,*B*) without changing sIPSC frequency ($\alpha1^{WT}$, 1.6 ± 0.3 Hz; n = 24; $\alpha1^{Mut}$, 1.1 ± 0.2 Hz; n = 25 cells; $p = 0.1220$, two-tailed unpaired *t* test).

The sIPSC kinetics were also altered with the half-decay time (T_{50}) increased for the α1 mutation ($\alpha1^{WT}$, 17.7 ± 1.5 ms, n = 21 cells; $\alpha1^{Mut}$, 26.2 ± 2 ms, n = 24; $p = 0.0016$, two-tailed unpaired *t* test), and the mean exponential decay time (τ) also increased ($\alpha1^{WT}$, 23.6 ± 2.3 ms; $\alpha1^{Mut}$, 37.5 ± 2.5 ms, n = 21-24; $p = 0.0002$, two-tailed unpaired *t* test). As a result of changes to sIPSC amplitudes and decay times, the charge transfer (median $\alpha1^{WT}$, −3221.5 pA.ms, n = 1306; $\alpha1^{Mut}$, −2817 pA.ms, n = 1330; $p <$ 0.001; Mann–Whitney test) was reduced for the $\alpha1^{Mut}$. By comparison, the sIPSC rise times ($\alpha1^{WT}$, 1.5 ± 0.1 ms, n = 21; $\alpha1^{Mut}$, 1.6 ± 0.1 ms, n = 24; $p = 0.7054$, two-tailed unpaired *t* test) remained unaffected.

Reduced sIPSC amplitudes could be due to several factors, including a dominant inhibitory effect of $\alpha1^{Mut}$ on the expression of WT GABA$_A$R subunits as noted for other epilepsy-inducing mutations of GABA$_A$Rs (Kang et al., 2009). However, maximal GABA-induced current densities were similar for hippocampal neurons expressing $\alpha1^{WT}$ or $\alpha1^{Mut}$ GABA$_A$Rs ($\alpha1^{WT}$: −71.6 ± 5.1 pA/pF, n = 45; $\alpha1^{Mut}$: −62 ± 3 pA/pF, n = 41; $p = 0.1196$, two-tailed unpaired *t* test; Fig. 6*C*,*D*), suggesting that overall cell surface expression per se of endogenous GABA$_A$R subunits remained affected by $\alpha1^{Mut}$. Nevertheless, using nonstationary noise analysis of peak-scaled sIPSCs, the mean number of α1-mutant GABA$_A$Rs activated at inhibitory synapses during the peak of the sIPSCs, compared with $\alpha1^{WT}$ neurons, was reduced (Fig. 6*E*,*F*; $\alpha1^{WT}$ 100.8 ± 20.3, n = 11; $\alpha1^{Mut}$ 44.2 ± 7.3, n = 9; $p = 0.0269$, two-tailed unpaired *t* test) without changing the single-channel conductance of synaptic GABA$_A$Rs ($\alpha1^{WT}$ 32.1 ± 8.5 pS, n = 11; $\alpha1^{Mut}$ 38.7 ± 8.7 pS, n = 9; $p = 0.5970$, two-tailed unpaired *t* test). Together, these results suggest that at the cell surface, specifically inhibitory synaptic membranes, $\alpha1^{Mut}$ directly affects receptor numbers and thus synaptic inhibitory current.

Evidence for α1-heteromeric GABA$_A$Rs

The impact of the α1 mutation on cell surface GABA$_A$R expression is most likely reflected by the sizeable reduction in sIPSC amplitude. However, the increased sIPSC decay constants

indicated that the mutation was also affecting receptor kinetics. We initially examined whether these effects may be caused by $\alpha1$ mutant subunits forming a pure population ($\alpha1^{Mut}\beta3\gamma2L$) contrasting with WT $\alpha1$ subunits expressed ($\alpha1^{WT}\beta3\gamma2L$) in separate pentamers. HEK-293 cells were transfected with cDNAs for $\alpha1^{WT}$ and/or $\alpha1^{Mut}$ (in equal ratio) with $\beta3$ and $\gamma2L$ and the resulting properties of the assembled receptors examined. Our initial premise was that hetero-$\alpha1$ subunit receptors might not form. Plotting the GABA concentration-response data and implementing Hill equation curve fits revealed four outcomes: the expected pure $\alpha1$-WT and pure $\alpha1$-mutant curves for HEK cells expressing separate $GABA_ARs$, and two relationships for cells expressing both $\alpha1^{WT}$ and $\alpha1^{Mut}$ with $\beta3\gamma2L$ (Fig. 7*A-C*). For the latter, GABA potency was reduced ninefold in ~11% of cells (EC_{50} = 87.3 ± 19 μM, n = 5; WT EC_{50} = 10.4 ± 1.7 μM, n = 14, $F_{(2, 57)}$ = 92.344, $p < 0.001$, one-way ANOVA, $p < 0.001$, *post hoc* Tukey-Kramer test, Fig. 7*A-C*; arbitrarily designated as Type 2), whereas the remainder had indistinguishable EC_{50}s from WT (EC_{50} = 8 ± 0.8 μM, n = 41; p = 0.796, Tukey-Kramer test, Fig. 7*A-C*; called Type 1). Moreover, the potency of Type 2 cells was lower compared with Type 1 cells ($p < 0.001$, Tukey-Kramer test).

The increased GABA EC_{50} in 11% of cells (Type 2) could represent the incorporation of $\alpha1^{Mut}$ into the same pentameric receptor with $\alpha1^{WT}$ and $\beta3\gamma2L$ subunits, especially given the different EC_{50}s (Fig. 7*A,B*), or conceivably, may reflect changes to the relative cell surface expression levels for pure pentamers of $\alpha1^{WT}\beta3\gamma2L$ and $\alpha1^{Mut}\beta3\gamma2L$.

To investigate whether the latter scenario could account for the change in GABA EC_{50}, we generated theoretical GABA concentration-response curves for pure $\alpha1$-WT and $\alpha1$-mutant receptor populations, assuming differential expression levels between 0% and 100%, with a maximum current set to 10% for $\alpha1^{Mut}$ compared with $\alpha1^{WT}$ receptors, and with EC_{50}s for $\alpha1^{Mut}$ and $\alpha1^{WT}$ taken from Figure 1. We explored varying the ratio of $\alpha1^{WT}$ to $\alpha1^{Mut}$ $GABA_ARs$ (keeping the total population constant) and normalizing the curves to the maximum response evoked by 50 mM GABA (Fig. 7*D*). Changing the proportion of $\alpha1^{WT}$ to $\alpha1^{Mut}$ between 0% and 100% revealed a family of curves with clear inflections especially when $\alpha1^{Mut}$ was the predominant receptor subunit (Fig. 7*D*), which became difficult to resolve when levels of $\alpha1^{WT}$ were increased (e.g., 50%).

To match the experimental (Type 2) EC_{50} of 87 μM for the $\alpha1^{WT}\alpha1^{Mut}$ $\beta3\gamma2L$ receptors, observed in 11% of cells, required a ~10%:90% ratio of $\alpha1^{WT}$:$\alpha1^{Mut}$. This seems unrealistic given that only 10% of mutant receptors reach the cell surface; and even if this occurred, the theoretical curves were clearly biphasic (Fig. 7*D*, green line), a feature not observed experimentally (Fig. 7*C*). Thus, determining one EC_{50} for the curve was inappropriate when two obvious components were present.

Given the mismatch of these simulations with the experimental data, we discarded the premise of pure $\alpha1$ subunit receptor populations and permitted coassembly of α subunits according to a binomial process. Simulated GABA concentration-response curves were generated initially based on a modified Hill equation (see

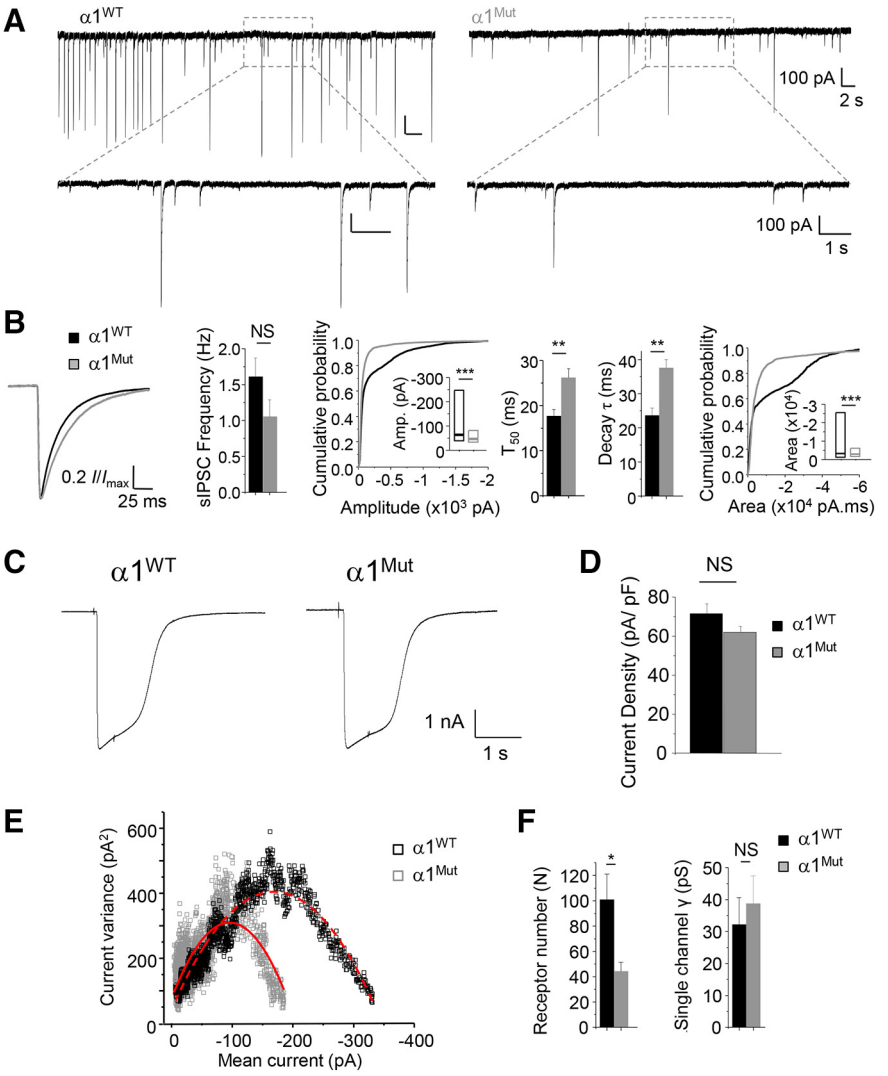

Figure 6. Mutant $\alpha1$ subunit-$GABA_ARs$ reduce sIPSC amplitudes. ***A***, Top, sIPSCs recorded from cultured hippocampal neurons clamped at −60 mV and expressing WT or mutant $\alpha1$-containing $GABA_ARs$. Bottom, Higher time resolution records from selected panels (dotted lines). ***B***, From left to right: Averaged sIPSC waveforms; sIPSC frequency and cumulative probability distribution of sIPSC amplitudes (inset: box plot showing median and 25%-75% interquartile range of amplitudes, Amp.); sIPSC half-decay time (T_{50}), exponential decay times, and cumulative distribution of area (charge transfer) (inset, box plot shows median and 25%-75% interquartile range of the sIPSC area), for WT and mutant $\alpha1$ subunit-containing $GABA_ARs$. $^{**}p < 0.01$ (two-tailed unpaired *t* test). n = 21-25 neurons for bar charts. $^{***}p < 0.001$ (Mann–Whitney test). n = 5236-5664 events for sIPSC cumulative amplitude distributions from 24-25 cells. n = 1306-1330 for sIPSC cumulative area distributions. ***C***, Whole-cell 1 mM GABA-activated currents recorded at −20 mV in neurons expressing $\alpha1^{WT}$ or $\alpha1^{Mut}$ $GABA_ARs$. ***D***, Mean GABA current densities for $\alpha1^{WT}$- and $\alpha1^{Mut}$-expressing neurons (n = 41-45 neurons). Two-tailed unpaired *t* test. ***E***, Nonstationary noise analysis for sIPSCs recorded from neurons expressing WT or mutant $GABA_ARs$. ***F***, Bar graphs of number of receptors (*N*) at inhibitory synapses activated during the peak sIPSC, and single-channel conductance of $GABA_ARs$. n = 9-11 neurons. NS, not significant; $^{*}p < 0.05$ (two-tailed unpaired *t* test).

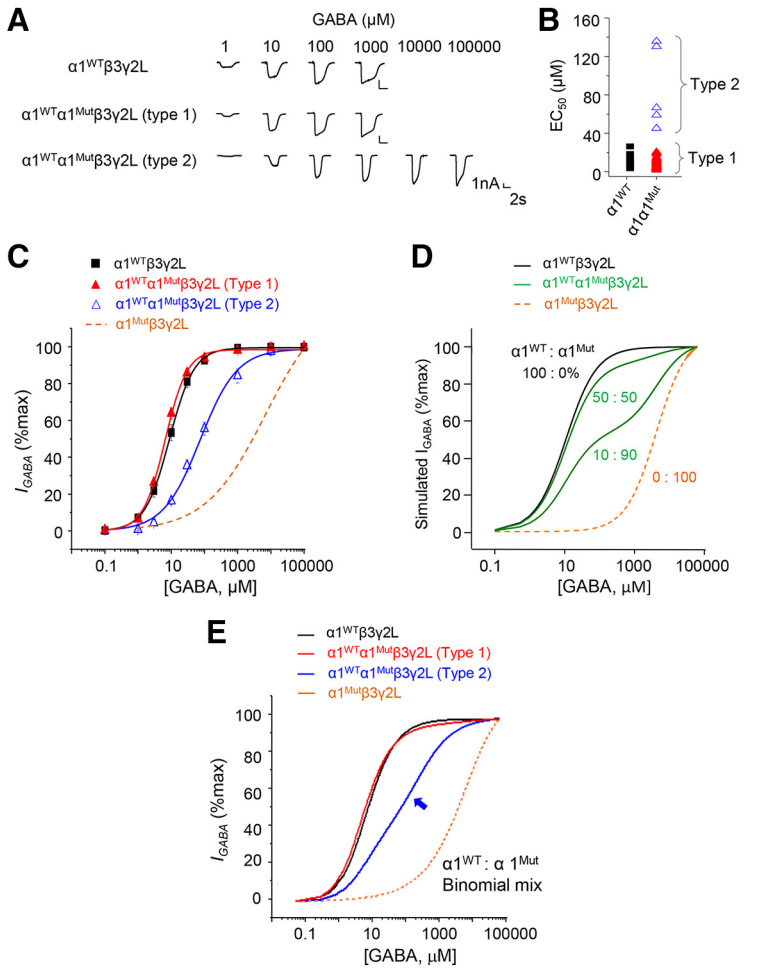

Figure 7. Formation of α1-heteromeric GABA$_A$Rs. ***A***, GABA-activated currents for pure and mixed α1 subunit-containing receptors expressed with β3γ2L in HEK-293 cells. ***B***, EC_{50} values are plotted for individual cells for pure and mixed α1 subunit-containing receptors. Arbitrarily defined Type 1 receptors have EC_{50}s similar to WT, and Type 2 receptors have ~eightfold higher EC_{50}s. ***C***, GABA concentration-response relationships for α1 WT and for cells expressing $\alpha1^{Mut}$ with α1 WT subunits: $n = 41$ for Type 1 receptors, 5 for Type 2 receptors, and 14 for WT receptors. The curve for $\alpha1^{Mut}\beta3\gamma2L$ is shown for comparison (orange dashed line) (data from Fig. 1*C*). ***D***, GABA concentration curves generated by a modified Hill equation based on expressing just two pure populations of receptors: $\alpha1^{WT}\beta3\gamma2L$ and $\alpha1^{Mut}\beta3\gamma2L$ with EC_{50}s (data from Fig. 1*C*). As $\alpha1^{Mut}$ receptors were trafficking-impaired, their access to the cell surface was limited to 10% of WT. The relative proportions (%) of $\alpha1^{WT}$ and $\alpha1^{Mut}$ were varied between curves from 100 ($\alpha1^{WT}$):0 ($\alpha1^{Mut}$)% (black line), to 50:50 and 10:90 (green), and 0:100 (orange dashed line). ***E***, Simulated GABA concentration-response curves for a binomial mixture of $\alpha1^{WT}$ and $\alpha1^{Mut}$ with β3 and γ2L subunits as indicated by the key. A binomial distribution was assumed to occur for assembly ($\alpha1^{WT}$ 25%, $\alpha1^{WT}\alpha1^{Mut}$ 50%, $\alpha1^{Mut}$ 25%) with trafficking to the cell surface as ($\alpha1^{WT}$ 54%, $\alpha1^{WT}\alpha1^{Mut}$ 40%, and $\alpha1^{Mut}$ 6%) with EC_{50}s and Hill slopes of ($\alpha1^{WT}$ 6.93 μM, 1.33; $\alpha1^{WT}\alpha1^{Mut}$ 87 μM, 0.79 [Type 2 blue curve], 3.58 μM, 1.63 [Type 1, red curve]; $\alpha1^{Mut}$ 10.7 mM, 0.56).

Materials and Methods) and the presence of $\alpha1^{WT}\beta3\gamma2L$, $\alpha1^{WT}\alpha1^{Mut}\beta3\gamma2L$, and $\alpha1^{Mut}$ $\beta3\gamma2L$ in approximate binomial proportions of 0.25:0.5:0.25. On this basis, the simulated curves accurately reflected the experimental data and predicted that the majority of receptors at the cell surface were $\alpha1^{WT}$-containing (54%), $\alpha1^{WT}\alpha1^{Mut}$-containing (40%), with the remainder (~6%) just $\alpha1^{Mut}$-containing. Furthermore, on the simulated curves for the $\alpha1^{WT}\alpha1^{Mut}$-containing receptors (Fig. 7*E*, blue line and arrow) an inflection is discernible, although this is hard to resolve in the experimental graphs without further data points, but it is a consequence of some pure $\alpha1^{Mut}$-containing receptors accessing the cell surface.

Thus, differential assembly and altered trafficking for the $\alpha1^{Mut}$ receptor will have an impact on the GABA concentration-response curves. Moreover, using confocal microscopy, the levels of cell expression of WT receptors do not change when coexpressed with mutant receptors (normalized surface expression levels: $\alpha1^{WT}$ – 100, $n = 38$; $\alpha1^{WT}$ + $\alpha1^{Mut}$ – 96.4 ± 3.2, $n = 42$; eGFP only – 1.5 ± 0.5, $n = 24$. $F_{(2, 101)} = 355.948$, $p < 0.001$, one-way ANOVA; $p = 0.553$ Tukey-Kramer *post hoc* WT vs WT and mutant receptors; Fig. 8*A*,*B*). Together, the most likely explanation for the change of GABA sensitivity in some HEK-293 cells is the incorporation of $\alpha1^{Mut}$ into the same pentameric complex with α1 subunits forming an α subunit hetero-pentamer with altered kinetic profile.

To explore the importance of the α1 subunit for synaptic inhibition, we used the imidazopyridine z-drug, zolpidem, which at 100 nM is a selective modulator of α1 subunit-containing GABA$_A$ receptors (Pritchett et al., 1989; Perrais and Ropert, 1999). Application of 100 nM zolpidem to neurons expressing $\alpha1^{WT}$ revealed prolongations of sIPSC decays as expected (Vicini et al., 2001), increasing both the T_{50} ($p = 0.0094$) and exponential decay τ ($p = 0.003$; Fig. 8*C*,*D*). Comparing this outcome with neurons expressing $\alpha1^{Mut}$-GABA$_A$Rs revealed two notable features. The sIPSC decay was prolonged (T_{50} and decay τ both $p < 0.001$; Fig. 8*C*,*E*), but not to the same extent as for $\alpha1^{WT}$ (56%-65% increase in T_{50} and τ for $\alpha1^{WT}$, and 28%-35% for $\alpha1^{Mut}$). Given that the truncation of the α1 subunit is unlikely to directly affect modulation of the receptor by zolpidem, the difference in sIPSC decay prolongations suggests α1 subunit GABA$_A$Rs are reduced in number at inhibitory synapses.

Overall, these results suggest that α1-mutant-containing GABA$_A$Rs are disrupting the expression of GABA$_A$Rs at inhibitory synapses.

Discussion

The advent of high-throughput sequencing heralds a new era for investigating the genetic basis of neurodevelopmental disorders. Whole exome sequencing has identified numerous mutations to genes encoding for ion channels and neurotransmitter receptors that underlie neurologic disorders (Foo et al., 2012). To understand how individual variants orchestrate pathologic features requires extensive neurobiological and biophysical characterization of ion channel and receptor dysfunction.

Genetic variants account for >40% of all epilepsies (Robinson and Gardiner, 2000) and structural modifications to several GABA$_A$R subunits, ranging from residue substitutions to substantive deletions and truncations, with or without frameshift insertions, alter many aspects of inhibitory signaling, including the following: GABA sensitivity (Hernandez et al., 2016), receptor activation/deactivation kinetics (Audenaert et al., 2006; Lachance-Touchette et al., 2011; Hernandez et al., 2016), sensitivity to ligands (Audenaert et al., 2006), ER retention (Kang and Macdonald, 2004; Lachance-Touchette et al., 2011), receptor degradation (Kang et al., 2015), assembly (Hales et al., 2005), and cell surface trafficking/expression

(Sancar and Czajkowski, 2004; Maljevic et al., 2006; Tian et al., 2013). All these features can contribute toward a catalog of generalized and partial seizures. For example, point mutations affecting $\alpha 1$ subunits associated with epilepsy variously reduce cell surface expression due to nonsense-mediated mRNA decay and ER-associated protein degradation (Gallagher et al., 2005; Kang and Macdonald, 2009). This can alter receptor kinetics and affect GABA sensitivity (Fisher, 2004; Galanopoulou, 2010). These changes can reduce inhibitory synaptic efficacy and reflect the importance of dysfunctional GABA signaling as a key mechanism in genetic epilepsy.

By characterizing a variant in the $GABA_AR$ $\alpha 1$ subunit that causes severe epilepsy, we have identified impaired signaling and cell surface expression of $GABA_ARs$ that are unusual in regard to epilepsy. At a molecular level, although the mutant $\alpha 1$ subunit lacks a substantive structural component, including part of the M3-M4 domain and all of M4, the mutant receptor still retains its signaling ability, albeit reduced, compared with WT receptors. The large reduction in GABA sensitivity (>400 fold) and maximal currents, including decreased receptor activation and slower deactivation, and reduced synaptic numbers of $GABA_A$ receptors, will all reduce the efficacy of inhibition imparted by this important subpopulation of synaptic $GABA_ARs$ (Galanopoulou, 2010). The combined effects of these defects masked the reduced desensitization we observed for the mutant, and also reduced charge transfer via synaptic $GABA_ARs$.

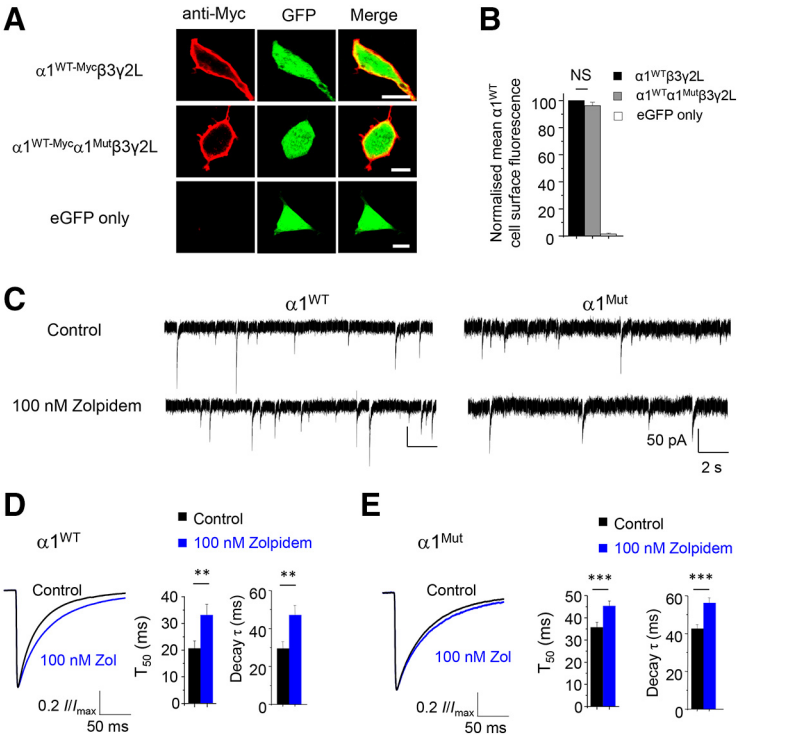

Figure 8. Expression of the $\alpha 1$ mutant subunits does not affect $\alpha 1$ subunit surface expression and potentiation of IPSCs by zolpidem. ***A***, Confocal images of cell surface labeling of WT $\alpha 1^{myc}$ $GABA_ARs$ in the absence (top row) or presence of coexpressed mutant $\alpha 1$ or eGFP only. Scale bars, 5 μm. ***B***, Mean fluorescence intensities for WT $\alpha 1$ $GABA_ARs$ in the absence and presence of mutant $\alpha 1$ or eGFP only. Data normalized to levels of $\alpha 1^{WT}$ myc staining. One-way ANOVA, $n = 24$-42. ***C***, Representative sIPSCs recorded from hippocampal neurons expressing $\alpha 1^{WT}$ or mutant $\alpha 1^{Mut}$-containing $GABA_ARs$ under control conditions or in the presence of 100 nM zolpidem. ***D***, ***E***, Average sIPSC waveforms, half-decay times (T_{50}), and decay τ in the presence of 100 nM zolpidem for $\alpha 1^{WT}$ (***D***) and $\alpha 1^{Mut}$ (***E***) expressing neurons. $n = 9$-12. NS, not significant; $^{**}p < 0.01$; $^{***}p < 0.001$; two-tailed paired *t* test.

The role of M4 is clearly important, but its loss does not prevent $\alpha 1^{Mut}$ assembly into the receptor. However, it does influence $\alpha\beta$ subunit incorporation. Our experiments using mammalian cells demonstrate that the truncated subunit preferentially associates with $\beta 3$ over $\beta 2$ subunits. In regard to their structure, β subunits are very highly conserved (Taylor et al., 2000; Sigel and Steinmann, 2012). Differential assembly and/or trafficking of the $\alpha 1$ mutants with β subunits might occur because losing M4 may alter α subunit conformation such that there is simply preferred assembly and/or cell surface trafficking with $\beta 3$ over $\beta 2$ subunits. It is clear that the GKER motif in the ECD of $\beta 3$ subunits is important for enabling expression of $\alpha 1^{Mut}$ containing receptors, but given that it has only a partial effect, it indicates that other domains in the $\beta 3$ subunit must also play important roles. The truncated portion of the $\alpha 1$-mutant subunit's large intracellular domain between M3 and M4 is unlikely to be directly important for this process as substituting the entire domain for a serine-glycine linker, or a *Gloeobacter violaceus* heptapeptide, affected neither the assembly, cell surface expression, nor dramatically affected signaling of $\alpha 1$ with $\beta 2$ subunits (Jansen et al., 2008; Hannan and Smart, 2018). The preference of $\alpha 1^{Mut}$ for $\beta 3$ over $\beta 2$ is subtle since assembly in *Xenopus* oocytes is seemingly unaffected by the loss of M4. This suggests that $\alpha 1^{Mut}$ and $\beta 2$ coassembly is slow and possibly inefficient, requiring longer incubation times that are afforded by using *Xenopus* oocytes compared with HEK cells. This highlights the importance of studying disease variants in mammalian, preferably native, systems. Whether the mutation affects cell surface trafficking and/or subunit coassembly may be determined from applying biochemical methods. Nevertheless, the overall outcome is clear: $\alpha 1^{Mut}$ reduces cell surface expression.

Given the reduced maximal GABA currents with the mutant receptors, we used flow cytometry to study $GABA_AR$ expression efficiency. Flow cytometry corroborated the electrophysiology findings revealing severely impaired cell surface trafficking for $\alpha 1$ mutant receptors, with preferential coexpression with $\beta 3$ over $\beta 2$ subunits. A similar profile emerged for receptor expression in neurons. The overall expression levels for WT and mutant $\alpha 1$ subunits (surface + intracellular) were identical in HEK-293 cells. The limited trafficking to the cell surface occurred as a result of substantive retention in the ER. This may result from the Lys373, in part, acting as a retention motif following truncation (Teasdale and Jackson, 1996). The 24 new amino acids contain two further Lys residues located at intervals of 7 or 8 residues, although these are not traditional retention motifs (Teasdale and Jackson, 1996). Nevertheless, the outcome of ER retention is that the functionally impaired $\alpha 1$ mutant is not expressed on the cell surface efficiently, and this will be a major determining factor in causing seizures as the efficacy of inhibition, imparted by the single WT allele, may not be adequate to control neuronal excitation.

The addition of the 24 *de novo* amino acids after Lys373 had no impact on $GABA_AR$ signaling since there was no difference in GABA sensitivity or receptor kinetics between $\alpha\beta\gamma$ receptors

incorporating either $\alpha1^{Mut}$ or $\alpha1^{\Delta373}$. The additional amino acids had only a minimal effect on cell surface expression of the mutant receptors as the truncation $\alpha1^{\Delta373}$ displayed a slightly greater area in Q2 flow cytometry compared with $\alpha1^{Mut}$, a feature that is unlikely to be significant for the seizure intensities observed in the individual harboring the genetic variant.

The first indication that $GABA_AR$ subunit composition may be affected by $\alpha1^{Mut}$ was evident from the large-amplitude reduction and increased decay kinetics for sIPSCs, which we postulated may occur following incorporation of mutant subunits into synaptic $GABA_ARs$. The reduced inhibitory transmission efficacy was not due to a dominant-negative effect on the expression of other WT subunits as whole-cell maximal GABA-activated current densities were unaffected. A reduction in receptor numbers at inhibitory synapses could explain the reduction in sIPSC amplitudes. Impaired lateral diffusion-mediated recruitment/retention of receptors at the synapse could also be due to the $\alpha1$ subunit mutation, accounting for the changed synaptic current profiles. This concept also accords with the zolpidem effects on the sIPSC decays. Prolongation by zolpidem signals that $\alpha1$ subunit $GABA_ARs$ are present at the inhibitory synapse, but this was clearly reduced by the presence of $\alpha1^{Mut}$. The simplest and also speculative explanation for this is that $\alpha1^{Mut}$ hinders the trafficking of the receptor to the synaptic membrane and could account for why sIPSC amplitudes are reduced, whereas GABA whole-cell currents are unaffected, as $\alpha1^{Mut}$ receptors remain mostly outside the synapse. It was also notable that the control sIPSC decays for $\alpha1^{Mut}$ are longer than for $\alpha1^{WT}$-expressing neurons. This may signify an effect of $\alpha1^{Mut}$ on kinetics and/or the influx of other α subunit $GABA_ARs$ (e.g., $\alpha2$) as part of a homeostatic mechanism.

As the mutant expression levels at the cell surface of transfected neurons equate to ~25% of WT subunit levels, but reduce sIPSC amplitudes by ~50%, this suggested that a disproportionately larger pool of receptors contain mutant $\alpha1$ subunits than expected. Furthermore, by modeling the concentration-response curves for mixtures of two separate populations of $GABA_ARs$ containing either $\alpha1^{WT}$ or $\alpha1^{Mut}$ subunits, with varying expression levels, it became clear that the widely separated EC_{50}s for $\alpha1^{WT}$ and $\alpha1^{Mut}$ should be reflected by easily detected biphasic curves. This was not observed experimentally, although the curves for $\alpha1^{WT}$ (EC_{50} ~10 μM) and $\alpha1^{Mut}$ (EC_{50} 3.8 mM) are separated by an ~380-fold shift. The curve for a mixture of $\alpha1^{WT}$ and $\alpha1^{Mut}$ (EC_{50} 87 μM) was seemingly monophasic, which could not be accounted for by differential levels of $\alpha1$ subunit expression, but could represent a heteromeric α subunit $GABA_AR$ composed of both $\alpha1^{WT}$ and $\alpha1^{Mut}$. Using a binomial model for coassembly does account for the GABA concentration-response curve profiles but requires most (~95%) of the $\alpha1$ subunit-containing receptors in the cell membrane to be either composed of $\alpha1^{WT}\beta3\gamma2L$ or $\alpha1^{WT}\alpha1^{Mut}\beta3\gamma2L$ receptors. This circumstance, whereby a pathologic mutation readily assembles as part of a heteromeric α subunit $GABA_AR$ complex, can also be diversified to include a preference for $\beta3$ over $\beta2$ subunit assembly.

Thus, these new findings suggest that, although the structure and expression profile of mutant $\alpha1$ subunits is significantly impaired, their low GABA sensitivity reduces the efficacy of synaptic inhibition of WT $\alpha1$-containing $GABA_ARs$ by coassembly in the same pentamer. This heteromeric coassembly not only adds an additional level of complexity to epilepsy-causing haploinsufficiency but also presents the likelihood that selected heteromeric (WT) α subunit receptors may be physiologically more prevalent in the brain than previously thought, adding to the structural diversity of neuronal $GABA_ARs$.

References

Audenaert D, Schwartz E, Claeys KG, Claes L, Deprez L, Suls A, Van DT, Lagae L, Van BC, Macdonald RL, De Jonghe P (2006) A novel GABRG2 mutation associated with febrile seizures. Neurology 67:687–690.

Connolly CN, Krishek BJ, McDonald BJ, Smart TG, Moss SJ (1996) Assembly and cell surface expression of heteromeric and homomeric γ-aminobutyric acid type-A receptors. J Biol Chem 271:89–96.

Datta D, Arion D, Lewis DA (2015) Developmental expression patterns of $GABA_A$ receptor subunits in layer 3 and 5 pyramidal cells of monkey prefrontal cortex. Cereb Cortex 25:2295–2305.

Fisher JL (2004) A mutation in the $GABA_A$ receptor $\alpha1$ subunit linked to human epilepsy affects channel gating properties. Neuropharmacology 46:629–637.

Foo JN, Liu JJ, Tan EK (2012) Whole-genome and whole-exome sequencing in neurological diseases. Nat Rev Neurol 8:508–517.

Galanopoulou A (2010) Mutations affecting GABAergic signaling in seizures and epilepsy. Pflugers Arch 460:505–523.

Gallagher MJ, Shen W, Song L, Macdonald RL (2005) Endoplasmic reticulum retention and associated degradation of a $GABA_A$ receptor epilepsy mutation that inserts an aspartate in the M3 transmembrane segment of the $\alpha1$ subunit. J Biol Chem 280:37995–38004.

Hales TG, Tang H, Bollan KA, Johnson SJ, King DP, McDonald NA, Cheng A, Connolly CN (2005) The epilepsy mutation, $\gamma2$ (R43Q) disrupts a highly conserved inter subunit contact site, perturbing the biogenesis of $GABA_A$ receptors. Mol Cell Neurosci 29:120–127.

Hannan S, Smart TG (2018) Cell surface expression of homomeric $GABA_A$ receptors depends on single residues in subunit transmembrane domains. J Biol Chem 293:13427–13439.

Hannan S, Wilkins ME, Thomas P, Smart TG (2013) Tracking cell surface mobility of GPCRs using α-bungarotoxin-linked fluorophores. Methods Enzymol 521:109–129.

Hannan S, Minere M, Harris J, Izquierdo P, Thomas P, Tench B, Smart TG (2020) $GABA_AR$ isoform and subunit structural motifs determine synaptic and extrasynaptic receptor localisation. Neuropharmacology 169:107540.

Hanrahan JW (2004) Cystic fibrosis transmembrane conductance regulator. Adv Mol Cell Biol 32:73–94.

Hernandez CC, Klassen TL, Jackson LG, Gurba K, Hu N, Noebels JL, Macdonald RL (2016) Deleterious rare variants reveal risk for loss of $GABA_A$ receptor function in patients with genetic epilepsy and in the general population. PLoS One 11:e0162883.

Hutcheon B, Fritschy JM, Poulter MO (2004) Organization of GABA receptor α subunit 26 clustering in the developing rat neocortex and hippocampus. Eur J Neurosci 19:2475–2487.

Jansen M, Bali M, Akabas MH (2008) Modular design of Cys-loop ligand-gated ion channels: functional 5-HT_3 and GABA $\rho1$ receptors lacking the large cytoplasmic M3-M4 loop. J Gen Physiol 131:137–146.

Kang JQ, Macdonald RL (2004) The $GABA_A$ receptor $\gamma2$ subunit R43Q mutation linked to childhood absence epilepsy and febrile seizures causes retention of $\alpha1\beta2\gamma2S$ receptors in the endoplasmic reticulum. J Neurosci 24:8672–8677.

Kang JQ, Macdonald RL (2009) Making sense of nonsense $GABA_A$ receptor mutations associated with genetic epilepsies. Trends Mol Med 15:430–438.

Kang JQ, Shen W, Macdonald RL (2009) The GABRG2 mutation, Q351X, associated with generalized epilepsy with febrile seizures plus, has both loss of function and dominant-negative suppression. J Neurosci 29:2845–2856.

Kang JQ, Shen W, Zhou C, Xu D, Macdonald RL (2015) The human epilepsy mutation GABRG2 (Q390X) causes chronic subunit accumulation and neurodegeneration. Nat Neurosci 18:988–996.

Lachance-Touchette P, Brown P, Meloche C, Kinirons P, Lapointe L, Lacasse H, Lortie A, Carmant L, Bedford F, Bowie D, Cossette P (2011) Novel $\alpha1$ and $\gamma2$ $GABA_A$ receptor subunit mutations in families with idiopathic generalized epilepsy. Eur J Neurosci 34:237–249.

Leach MR, Williams DB (2011) Calnexin and calreticulin, molecular chaperones of the endoplasmic reticulum. In: Calreticulin: molecular biology intelligence unit (Eggleton P, Michalak M, eds). Boston: Springer.

Macdonald RL, Gallagher MJ, Feng HJ, Kang J (2004) $GABA_A$ receptor epilepsy mutations. Biochem Pharmacol 68:1497–1506.

Maljevic S, Krampfl K, Cobilanschi J, Tilgen N, Beyer S, Weber YG, Schlesinger F, Ursu D, Melzer W, Cossette P, Bufler J, Lerche H, Heils A (2006) A mutation in the $GABA_A$ receptor α1 subunit is associated with absence epilepsy. Ann Neurol 59:983–987.

Maljevic S, Møller RS, Reid CA, Pérez-Palma E, Lal D, May P, Lerche H (2019) Spectrum of $GABA_A$ receptor variants in epilepsy. Curr Opin Neurol 32:183–190.

Mann EO, Paulsen O (2007) Role of GABAergic inhibition in hippocampal network oscillations. Trends Neurosci 30:343–349.

Mitchell SJ, Silver RA (2003) Shunting inhibition modulates neuronal gain during synaptic excitation. Neuron 38:433–445.

Perrais D, Ropert N (1999) Effect of zolpidem on miniature IPSCs and occupancy of postsynaptic $GABA_A$ receptors in central synapses. J Neurosci 19:578–588.

Popp B, Trollmann R, Büttner C, Caliebe A, Thiel CT, Hüffmeier U, Reis A, Zweier C (2016) Do the exome: a case of Williams-Beuren syndrome with severe epilepsy due to a truncating de novo variant in GABRA1. Eur J Med Genet 59:549–553.

Pritchett DB, Lüddens H, Seeburg PH (1989) Type I and type II $GABA_A$-benzodiazepine receptors produced in transfected cells. Science 245:1389–1392.

Robinson R, Gardiner M (2000) Genetics of childhood epilepsy. Arch Dis Child 82:121–125.

Sancar F, Czajkowski C (2004) A $GABA_A$ receptor mutation linked to human epilepsy (γ2R43Q) impairs cell surface expression of $\alpha\beta\gamma$ receptors. J Biol Chem 279:47034–47039.

Sieghart W, Sperk G (2002) Subunit composition, distribution and function of $GABA_A$ receptor subtypes. Curr Top Med Chem 2:795–816.

Sigel E, Steinmann ME (2012) Structure, function, and modulation of $GABA_A$ receptors. J Biol Chem 287:40224–40231.

Smart TG, Krishek BJ (1995) Xenopus oocyte microinjection and ion-channel expression. In: Patch-clamp applications and protocols (Boulton AA, Baker GB, Walz W, eds), Vol 26. Totowa, NJ:Humana Press.

Taylor PM, Connolly CN, Kittler JT, Gorrie GH, Hosie A, Smart TG, Moss SJ (2000) Identification of residues within $GABA_A$ receptor α subunits that mediate specific assembly with receptor β subunits. J Neurosci 20:1297–1306.

Taylor PM, Thomas P, Gorrie GH, Connolly CN, Smart TG, Moss SJ (1999) Identification of amino acid residues within $GABA_A$ receptor β subunits that mediate both homomeric and heteromeric receptor expression. J Neurosci 19:6360–6371.

Teasdale RD, Jackson MR (1996) Signal-mediated sorting of membrane proteins between the endoplasmic reticulum and the Golgi apparatus. Annu Rev Cell Dev Biol 12:27–54.

Thomas P, Smart TG (2012) Use of electrophysiological methods in the study of recombinant and native neuronal ligand-gated ion channels in the study of recombinant and native neuronal ligand-gated ion channels. Curr Protoc Pharmacol 59:11.4.1.

Tian M, Mei D, Freri E, Hernandez CC, Granata T, Shen W, Macdonald RL, Guerrini R (2013) Impaired surface $\alpha\beta\gamma$ $GABA_A$ receptor expression in familial epilepsy due to a GABRG2 frameshift mutation. Neurobiol Dis 50:135–141.

Vicini S, Ferguson C, Prybylowski K, Kralic J, Morrow AL, Homanics GE (2001) $GABA_A$ receptor α1 subunit deletion prevents developmental changes of inhibitory synaptic currents in cerebellar neurons. J Neurosci 21:3009–3016.

Whiting PJ (2003) $GABA_A$ receptor subtypes in the brain: a paradigm for CNS drug discovery? Drug Discov Today 8:445–450.